Published by Avanti Publishers

Journal of Advanced Thermal Science Research

ISSN (online): 2409-5826


# Magneto-Radiative Slip Flow of Couple Stress Cu–$Al_2O_3$ Hybrid Nanofluid over a Stretching Sheet with Activation Energy

Samir K. Nandy[1,*], Rajib K. Mandal[2] and Shampa Mondal[2]

[1]*Department of Mathematics, A.K.P.C. Mahavidyalaya, Bengai, Hooghly-712611, India*
[2]*Department of Physics, A.K.P.C. Mahavidyalaya, Bengai, Hooghly-712611, India*

## ARTICLE INFO

*Article Type*: Research Article

*Academic Editor*: Dunxi Yu

*Keywords*:
Thermal radiation effects
Couple stress hybrid nanofluid
Stretching sheet boundary layer
Magnetohydrodynamic (MHD) flow
Activation energy and mass transfer

*Timeline*:
Received: October 06, 2025
Accepted: November 25, 2025
Published: December 29, 2025

*Citation*: Nandy SK, Mandal RK, Mondal S. Magneto-radiative slip flow of couple stress Cu–$Al_2O_3$ hybrid nanofluid over a stretching sheet with activation energy. J Adv Therm Sci Res. 2025; 12: 170-193.

*DOI*: https://doi.org/10.15377/2409-5826.2025.12.10

## ABSTRACT

This research focuses on enhancing heat transfer performance through the use of a couple stress hybrid nanofluid, representing a notable advancement in nanofluid-based thermal technologies. A mixture of copper (Cu) and aluminum oxide ($Al_2O_3$) nanoparticles is dispersed in a base fluid composed of equal proportions of ethylene glycol and water, forming a hybrid nanofluid selected for its enhanced thermal conductivity and suitability for industrial applications such as cooling devices, refrigeration systems, and food processing operations. This study investigates the influence of several key factors—namely first-order velocity slip, magnetic field effects, internal heat generation/absorption, thermal radiation and activation energy—on the flow, thermal and concentration characteristics of the nanofluid. The analysis is carried out by converting the governing partial differential equations into nonlinear ordinary differential equations via similarity transformations, followed by numerical integration using MATLAB's ode45 solver. Results are presented graphically to illustrate the influence of varying physical parameters on the hydrodynamic, thermal, and concentration characteristics. It is observed that an increase in magnetic field strength suppresses the fluid velocity due to the action of the Lorentz force, while simultaneously enhancing the temperature and concentration fields. Similarly, greater values of the couple stress parameter lead to an increase in fluid velocity and a simultaneous reduction in temperature and concentration. In addition, the concentration profile is found to improve significantly with higher activation energy. An increase in the magnetic parameter and the couple stress parameter restrains fluid motion and reduces the thickness of the thermal boundary layer, which in turn produces a sharper temperature gradient at the wall. This study offers valuable insights into optimizing thermal systems by manipulating flow and thermal parameters within couple stress hybrid nanofluids.

*Corresponding Author
Email: nandysamir@yahoo.com
Tel: +(91) 94 34667221

# 1. Introduction

## 1.1. Literature Review

Boundary-layer flow over stretching surfaces plays a crucial role in various industrial processes, such as extrusion, wire drawing, glass forming, and fibre production. In these operations, materials are extruded and stretched to attain the desired thickness, with the final product properties largely determined by the stretching rate and cooling conditions. Motivated by such practical considerations, Sakiadis [1] conducted the pioneering analysis of boundary-layer flow past a moving solid surface. Several subsequent studies have further advanced this field, as documented in Refs [2-5].

In numerous technological and industrial applications, non-Newtonian fluids are often favoured over Newtonian fluids due to their distinctive and adaptable flow properties. Unlike Newtonian fluids, their behaviour cannot be described by a single linear relationship between shear stress and shear rate; instead, their response varies with the flow conditions, making their characterization more complex. Non-Newtonian fluids play an essential role in areas such as polymer processing, food engineering, and printing technologies [6, 7]. To represent their diverse rheological behaviour, various constitutive models have been proposed, including the Power-law, Williamson, Jeffrey, Carreau, Cassonand Couple stress models.

Couple stress fluid theory is required to describe the behaviour of fluids that possess microstructure and exhibit size-dependent effects that cannot be captured by the classical Newtonian framework. In many practical systems—such as polymeric suspensions, biological fluids, lubricants, and flows through micro- and nano-scale channels—the internal rotation of fluid particles and the associated micro-level interactions play a significant role in the overall flow behaviour. Classical continuum theory neglects these micro-rotational effects and assumes a symmetric stress tensor, which becomes inadequate when the characteristic length of the flow domain approaches the molecular or microstructural length scale. To overcome this limitation, couple stress theory introduces a non-symmetric stress tensor along with a couple stress tensor that accounts for internal moments per unit area. This formulation incorporates an additional material length-scale parameter that reflects the influence of microstructure on momentum transport. As a result, couple stress fluids exhibit unique properties such as the presence of microrotation, higher-order velocity gradients, modified shear stress distributions, and enhanced resistance to deformation in thin film and confined flows. These features make couple stress theory particularly effective for accurately modelling microfluidics, lubrication processes, and complex fluids where rotational interactions and size effects are significant [8, 9]

Ali *et al*. [10] analysed unsteady MHD flow and heat transfer of couple-stress fluid over an oscillatory stretching sheet embedded in a porous medium and examined how couple-stress parameter affects velocity, skin friction and Nusselt number. Unsteady free-convective boundary layer flow of a couple-stress fluid over a stretching sheet with heat transfer was considered by Kumar *et al*. [11]. In another paper, thermal characteristics of couple stress fluid over an exponential stretching sheet was investigated by Shah *et al*. [12]. Very recently, the convective heat transfer characteristics of a couple-stress fluid, flowing along a shrinking surface under the influence of thermal radiation was considered by Hanif *et al*. [13]. They reported dual solutions within specific parameter ranges, and their results offer enhanced insight into the stability and thermal performance of non-Newtonian couple stress fluids.

One promising direction involves the use of nanoparticles—such as metallic particles (Cu, Ag, $Al_2O_3$), non-metallic particles ($SiO_2$, $TiO_2$), and carbon-based materials (graphene, carbon nanotubes, nanodiamonds)—dispersed in conventionally low-thermal-conductivity fluids, including water, ethylene glycol, engine oils, ethanol and various polymer solutions. These specially engineered fluids, called nanofluids, show much better heat transfer performance because of higher thermal conductivity, Brownian motion of the particles, and enhanced micro-convection at the fluid–particle interface. The term “nanofluid” was first introduced by Choi and Eastmann [14], who is widely recognized as a pioneer in this field. Since then, a growing number of researchers have investigated nanofluids from both experimental and theoretical perspectives, developing advanced models and numerical approaches for optimizing heat transfer, improving stability and predicting nanofluid behaviour across

a range of practical applications such as cooling of electronic devices, solar collectors, heat exchangers and biomedical systems [15-19].

In recent years, hybrid nanofluids have emerged as an advanced alternative to conventional single-component nanofluids due to their superior thermophysical properties and broader application potential. While traditional nanofluids employ a single type of nanoparticle—such as $Al_2O_3$, CuO, $TiO_2$, $SiO_2$ or graphene—to enhance the thermal conductivity of base fluids, their performance is often limited by factors such as particle agglomeration, saturation of thermal enhancement, and restricted tunability of rheological characteristics. Hybrid nanofluids overcome these limitations by dispersing two or more different nanoparticles—such as $Al_2O_3$–Cu**,** $TiO_2$–$SiO_2$**,** CuO–graphene, or Ag–CNT—within the same base fluid, enabling synergistic effects that significantly improve thermal conductivity, heat transfer rates, stability and energy transport capability. For example, $Al_2O_3$–Cu/water hybrid nanofluid exhibits higher thermal conductivity than either $Al_2O_3$/water or Cu/water nanofluids alone, while $TiO_2$–$SiO_2$/ethylene glycol hybrid nanofluid offers improved viscosity–conductivity balance for thermal systems. These enhanced characteristics make hybrid nanofluids particularly advantageous in high-performance heat exchanger systems, solar thermal devices, electronic cooling, automotive thermal management, and industrial processes where optimized heat transfer and stable suspensions are critical [20-23].

Gul *et al.* [24] investigated the flow and heat-transfer characteristics of a hybrid nanofluid composed of CuO–Cu nanoparticles over an inclined, slippery stretching surface**,** where the base fluid is modelled as a Casson fluid with an added couple-stress term**.** Their analysis incorporated nonlinear convection together with thermal radiation**,** providing important insight into hybrid nanofluid behavior under non-Newtonian and slip conditions**.** In a related contribution, Khashi'ie *et al.* [25] examined magnetohydrodynamic (MHD) couple-stress hybrid nanofluid flow over a convectively heated stretching sheet**,** highlighting the combined roles of magnetic field effects, convective boundary conditions, and couple-stress rheology on heat and momentum transport. Madhu [26] extended the analysis of couple-stress fluids by considering a 3D stretching-sheet geometry**,** where the impacts of viscous dissipation and Joule heating on couple-stress nanofluid flow were explored in detail. More recently, Khashi'ie *et al.* [27] performed a sensitivity analysis of MHD couple-stress hybrid nanofluid flow over a stretchable plate containing AA7072/AA7075 hybrid nanoparticles dispersed in methanol, emphasizing how variations in magnetic field strength, couple-stress parameter, and nanoparticle volume fraction significantly influence skin friction and heat-transfer rates. Collectively, these studies demonstrate the growing interest in hybrid nanofluid and couple-stress models for characterizing complex thermal–fluid interactions over stretching surfaces.

Magnetohydrodynamic (MHD) flow over a stretching sheet has extensive engineering and industrial applications due to its ability to control fluid motion, heat transfer, and boundary-layer behaviour using externally applied magnetic fields. In thermal engineering, the application of a magnetic field to electrically conducting fluids, such as hybrid nanofluids, provides a powerful means of controlling heat transfer and fluid flow over deformable or moving surfaces, such as stretching sheets encountered in polymer extrusion, thin-film coating, and material processing. The applied magnetic field produces a Lorentz force that resists the fluid flow, alters the momentum boundary layer, increases viscous dissipation, and leads to a thicker thermal boundary layer. Hybrid nanofluids, containing multiple types of nanoparticles, enhance the fluid's thermal conductivity and convective heat transfer compared to conventional fluids, while the magnetic field allows non-mechanical, externally adjustable control of flow, temperature, and nanoparticle distribution. Such MHD-assisted hybrid nanofluid flows over stretching sheets have practical significance in industrial cooling systems, electronic device thermal management, chemical reactors, polymer and metal processing, and microfluidic devices, where precise regulation of heat flux, cooling rate, and material uniformity is crucial. Studies have shown that by tuning the magnetic field strength, engineers can optimize skin friction, Nusselt number, and nanoparticle concentration profiles, enabling improved process efficiency and product quality without modifying the system's geometry or mechanical components. Numerous works have investigated these effects, demonstrating the practical and theoretical importance of MHD control in stretching-sheet flows [28-32].

In engineering mathematics, thermal radiation and activation energy are often integrated into mathematical models of heat and mass transfer, fluid flow, and reactive processes to accurately simulate real-world engineering systems. Thermal radiation is included in energy equations, typically through the Rosseland approximation or radiative heat flux models, to account for energy transfer by electromagnetic waves, especially at high

temperatures or in systems where conduction and convection alone are insufficient. By incorporating radiation terms, engineers can predict temperature distributions, thermal boundary-layer thickness, and heat flux more accurately, which is essential for processes like polymer extrusion, glass manufacturing, high-temperature reactors, and solar thermal systems. Activation energy is included in reaction rate terms in species or concentration equations, often using Arrhenius-type expressions, to represent the minimum energy required for chemical reactions to occur. In engineering mathematics, this allows the modeling of temperature-dependent reaction rates, which is critical for chemical reactors, catalytic processes, combustion systems, and polymerization reactions. By incorporating activation energy into differential equations governing mass transfer, engineers can predict species concentrations, reaction rates, and the influence of temperature or thermal fields on chemical processes.

Early investigations focused on the fluid flow of non-Newtonian fluids, such as Casson nanofluids, while accounting for porous media and chemical reactions, revealing the significant influence of magnetic fields, radiation, and reaction parameters on boundary-layer development, temperature distribution, and skin friction [33, 34]. MHD nanofluid flows incorporating thermal radiation, viscous dissipation, and internal heat generation or absorption over stretching sheets, which established the foundational methodology of governing partial differential equations, similarity transformations, and numerical solution techniques, were analyzed by Reddy *et al*. [35] and Daniel *et al*. [36]. More recently, research has focused on hybrid and tetra-hybrid nanofluids, integrating multiple nanoparticles with multi-physical effects including thermal radiation, activation-energy-dependent chemical reactions, non-uniform heat sources, and slip or transpiration boundary conditions to better represent practical engineering scenarios [37, 38]. These studies indicate that the application of magnetic fields tends to suppress fluid motion, while hybrid nanoparticles and radiative effects enhance convective heat transfer, offering potential for optimized thermal management. Collectively, the literature demonstrates a clear evolution from simplified MHD nanofluid models to comprehensive, multi-parameter frameworks capable of accurately predicting flow and heat transfer behaviour in engineering and industrial systems.

### 1.2. Significance of the Model

The couple stress fluid model is employed to account for microstructural and size-dependent effects induced by nanoparticles in hybrid nanofluids. This model is particularly relevant to biomedical applications, such as blood-based nanofluids and magnetic hyperthermia, where microscale rotational interactions significantly influence flow and thermal behaviour.

In magnetohydrodynamic (MHD) flows, the inclusion of couple stress effects enhances the modeling of momentum and heat transport under Lorentz force action. The couple stress parameter represents particle rotation, microscale torque, and non-Newtonian characteristics that become prominent at high nanoparticle concentrations and small length scales.

For microscale heat transfer applications, the model enables improved prediction of velocity and temperature fields compared to classical Newtonian formulations, ensuring a more realistic representation of hybrid nanofluid behaviour in biomedical, MHD, and advanced thermal systems.

### 1.3. Research Gap and Novelty

Although extensive research has been conducted on nanofluid flows over stretching sheets, very few studies have comprehensively investigated the combined effects of MHD, velocity slip, thermal radiation, and activation-energy-dependent chemical reactions in Couple Stress hybrid nanofluids**.** Most existing works treat these effects separately or focus on single nanofluids, thereby overlooking the complex multi-physical interactions that are critical for advanced industrial applications, including polymer extrusion, thin-film coating, chemical reactors, and electronic cooling systems. The novelty of the present study lies in developing a robust and comprehensive mathematical model that simultaneously accounts for non-Newtonian Couple Stress behaviour, hybrid nanoparticles, MHD, thermal radiation, and activation energy, along with the velocity slip boundary condition. This framework enables a thorough and systematic analysis of velocity, temperature, and concentration fields, providing valuable insights for optimizing heat and mass transfer, enhancing thermal management, and improving efficiency in a wide range of engineering and industrial processes.

## 2. Mathematical Formulation

We examine steady, two-dimensional slip flow of a viscous, electrically conducting couple-stress hybrid nanofluid past a stretching surface located at *y*=0, assuming incompressibility and the Boussinesq approximation. In the present model, the hybrid nanofluid consists of Copper (Cu) and Aluminum Oxide ($Al_2O_3$) nanoparticles suspended in a base fluid made of an equal mixture of ethylene glycol and water (50:50). The flow geometry is shown in Fig. (**1**), where the x-axis follows the direction of the flow and the y-axis is perpendicular to the stretching sheet. The fluid occupies the region y>0. A uniform magnetic field $B_0(x)$ is applied perpendicular to the stretching sheet. The surface temperature and concentration are denoted by $T_w$ and $C_w$, respectively while the ambient temperature and concentration far from the sheet are $T_\infty$ and $C_\infty$. It is assumed that $T_w > T_\infty$ and $C_w > C_\infty$.

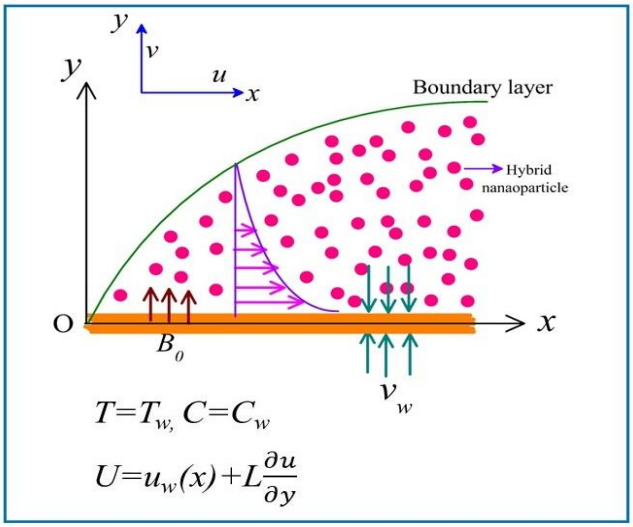


**Figure 1:** Physical model of the flow problem.

In view of the above assumptions, and by invoking the conventional boundary-layer approximations, the governing equations for the MHD flow, heat transfer, and mass transport of the couple-stress hybrid nanofluid can be expressed as follows [39, 40];

$$\frac{\partial u}{\partial x}+\frac{\partial v}{\partial y}=0 \tag{1}$$

$$u\frac{\partial u}{\partial x}+v\frac{\partial u}{\partial y}=\frac{\mu_{hnf}}{\rho_{hnf}}\frac{\partial^2 u}{\partial y^2}-\frac{\eta_0}{\rho_{hnf}}\frac{\partial^4 u}{\partial y^4}-\frac{\sigma_{hnf}}{\rho_{hnf}}B_0{}^2 u \tag{2}$$

$$u\frac{\partial T}{\partial x}+v\frac{\partial T}{\partial y}=\frac{\kappa_{hnf}}{\rho_{hnf}}\frac{\partial^2 T}{\partial y^2}+\frac{Q}{\left(\rho C_p\right)_{hnf}}\left(T-T_\infty\right)-\frac{1}{\left(\rho C_p\right)_{hnf}}\frac{\partial Q_n}{\partial y} \tag{3}$$

$$u\frac{\partial C}{\partial x}+v\frac{\partial C}{\partial y}=D_B\frac{\partial^2 C}{\partial y^2}-K_r{}^2\left(\frac{T}{T_\infty}\right)^n e^{-\frac{E_a}{K_T}}\left(C-C\infty\right) \tag{4}$$

Here, u and v denote the velocity components of the couple-stress hybrid nanofluid in the x- and y-directions, respectively; T represents the temperature, and C denotes the species concentration. The quantities $\mu_{hnf}$ and $\rho_{hnf}$ represent the dynamic viscosity and density of the hybrid nanofluid, respectively, while $\kappa_{hnf}$ denotes the

thermal conductivity and $(\rho C_p)_{hnf}$ corresponds to the effective heat capacity. The parameter $\eta_0$ denotes the couple-stress viscosity. The first term on the right hand side of (3) is due to thermal diffusivity, second term accounts for the heat source or sink and the last term is due to thermal radiation, whereas the last term on the right-hand side of equation (4) arises due to the activation energy.

The influence of the induced magnetic field is neglected because the magnetic Reynolds number ($R_M$) is very small. This approximation is well supported by laboratory evidence [41]. For typical hybrid nanofluid and couple-stress fluid flows characterized by moderate velocities and length scales, $R_M$ typically lies between $10^{-3}$ and $10^{-5}$, confirming that the induced magnetic field is negligible compared with the applied magnetic field.

The implemented boundary conditions for the problem are given by [39, 40]

$$u = u_w(x) + L\frac{\partial u}{\partial y}, v = v_w, T = T_w, C = C_w \text{ at y=0} \tag{5}$$

$$u \to 0, \frac{\partial u}{\partial y} \to 0, \frac{\partial^2 u}{\partial y^2} \to 0, T \to T_\infty, C \to C_\infty \text{ as } y \to \infty \tag{6}$$

where $u_w(x)=ax$ ($a>0$) is stretching sheet velocity, $L$ is the velocity slip factor, $v_w$ is the suction/injection parameter. It is essential to point out that boundary condition incorporates slip velocity which is significant in controlling the fluid characteristics.

The radiative heat flux is modeled using the Rosseland approximation [42, 43], given by $Q_n = -\frac{4\sigma^*}{3\kappa^*}\frac{\partial T^4}{\partial y}$ where $\sigma^*$ is the Stefan-Boltzmann constant and $\kappa^*$ is the mean absorption coefficient. Assuming the temperature variation is small, $T^4$ can be expanded in a Taylor series around $T_\infty$ and higher-order terms are ignored, yielding: $T^4 \approx 4T_\infty{}^3 T - 3T_\infty{}^4$.

So we have, $Q_n = -\frac{16\sigma^* T_\infty{}^3}{3\kappa^*}\frac{\partial^2 T}{\partial y^2}$.

For a steady, two-dimensional laminar boundary-layer flow of an incompressible hybrid nanofluid over a linearly stretching sheet, with negligible pressure gradient and induced magnetic field, appropriate similarity variables are introduced. These transformations reduce the governing momentum and energy equations, including MHD and couple-stress effects, to a system of ordinary differential equations under self-similar boundary conditions. This approach preserves the essential physical characteristics of the flow and heat transfer while simplifying the mathematical analysis.

Let us introduce the subsequent similarity variables [39, 40];

$$u = axf'(\eta),\ v = \sqrt{av_f}\,f(\eta),\ \theta(\eta) = \frac{T - T_\infty}{T_w - T_\infty},\ \phi(\eta) = \frac{C - C_\infty}{C_w - C_\infty} \text{ where } \eta = \sqrt{\frac{a}{\nu_f}}y \tag{7}$$

Equation (7) will be used to convert the equation (2)–(4) with boundary conditions (5)- (6) .

$$\frac{\mu_{hnf}/\mu_f}{\rho_{hnf}/\rho_f} f''' + ff'' - f'^2 - \frac{\rho_f}{\rho_{hnf}}\, k * f(v) - \frac{\sigma_{hnf}/\sigma_f}{\rho_{hnf}/\rho_f} Mf' = 0 \tag{8}$$

$$\frac{1}{Pr}\left(\frac{\kappa_{hnf}}{\kappa_f}+\frac{4}{3}R\right)\theta''+\frac{\left(\rho C_p\right)_{hnf}}{\left(\rho C_p\right)_f}f\theta'+\lambda\theta=0 \tag{9}$$

$$\frac{1}{Sc}\phi''+f\phi'-\Omega(\theta\gamma+1)^n.e^{-\frac{E}{(\theta\gamma+1)}}\phi=0 \tag{10}$$

The boundary conditions are

$$f\left(\eta\right)=S,\ f'\left(\eta\right)=1+\beta f''\left(\eta\right),\ \theta\left(\eta\right)=1,\ \phi\left(\eta\right)=1 \text{ at } \eta=0$$

$$f'(\eta)\to 0, f''\to 0, f'''\to 0, \theta(\eta)\to 0, \phi(\eta)\to 0 \ as\ \eta\to\infty \tag{11}$$

The parameters associated with the problems are:

The couple stress parameter $k^*\left(=\frac{\eta_0 a}{\mu_f \nu_f}\right)$, magnetic parameter $M\left(=\frac{\sigma_f B_0^{\ 2}}{a\rho_f}\right)$

The Prandtl number $Pr\left(=\frac{\left(\rho_{cp}\right)_f \nu_f}{K_f}\right)$, the heat source/sink parameter $\lambda\left(=\frac{Q}{a\left(\rho_{cp}\right)_f}\right)$, the Schmidt number $Sc\left(\frac{\nu_f}{D_B}\right)$,the chemical reaction parameter $\Omega\left(=\frac{K_r^{\ 2}}{a}\right)$, the activation energy $E\left(=\frac{E_a}{K}\right)$, the suction/injection parameter $S=-\frac{v_w}{\sqrt{a\nu_f}}$, the velocity slip parameter $\beta\left(=L\sqrt{\frac{a}{\gamma_f}}\right)$. The correlations for calculating hybrid nanofluid properties are listed in Table **1** [44, 45].

**Table 1: Correlations for hybrid nanofluids.**

| Properties | Hybrid Nanofluids |
|---|---|
| Density ( $\rho$) | $\rho_{hnf}=\left(1-\phi_{hnf}\right)\rho_f+\phi_1\rho_{s1}$ |
| Heat Capacity $\left(\rho C_p\right)$ | $:\left(\rho C_p\right)_{hnf}=\left(1-\phi_{hnf}\right)\left(\rho C_p\right)_f+\phi_1\left(\rho C_p\right)_{s1}+\phi_2\left(\rho C_p\right)_{s2}$ |
| Dynamic Viscosity ($\mu$) | $\frac{\mu_{hnf}}{\mu_f}=\frac{1}{\left(1-\phi_{hnf}\right)^{2.5}}$ |
| Thermal conductivity ($\kappa$) | $\frac{\kappa_{hnf}}{\kappa_f}=\left[\frac{\left(\frac{\phi_1\kappa_1+\phi_2\kappa_2}{\phi_{hnf}}\right)+2\kappa_f+2(\phi_1\kappa_1+\phi_2\kappa_2)-2\phi_{hnf}\kappa_f}{\left(\frac{\phi_1\kappa_1+\phi_2\kappa_2}{\phi_{hnf}}\right)+2\kappa_f-(\phi_1\kappa_1+\phi_2\kappa_2)+\phi_{hnf}\kappa_f}\right]$ |

The thermophysical properties of the base fluids and nanoparticles used in this study are summarized in Table **2** [44, 45].

**Table 2: Thermo physical properties of $Al_2O_3$, $Cu$ and $H_2O, EG$.**

| Thermo Physical Properties | Base Fluids | | Nanoparticles | |
|---|---|---|---|---|
| | $H_2O$ | EG | $Al_2O_3(\phi_1)$ | Cu ($\phi_2$) |
| $C_p$ | 4179 | 2400 | 765 | 385 |
| $\kappa$ | 0.613 | 0.258 | 40 | 400 |
| $\rho$ | 997.1 | 1190 | 3970 | 8933 |

Important measurable quantities in this study include the skin friction coefficient, the Nusselt number, and the Sherwood number. These parameters are crucial for characterizing flow behaviour and heat–mass transfer. They are widely used by engineers and scientists to improve system performance, optimize designs, and solve heat and mass transfer problems, thus supporting progress in engineering and technology. In practical engineering applications, the quantities $Cf_x, Nu_x$, and $Sh_x$ denote the local skin friction coefficient, the local Nusselt number, and the local Sherwood number, respectively, each defined by the corresponding expressions:

$$Cf_x = \frac{\tau_\omega}{\frac{1}{2}\rho u^2{}_e}, \quad Nu_x = \frac{xq_\omega}{k_f\left(T_w - T\infty\right)}, \quad Sh_x = \frac{xq_m}{D_B\left(C_w - C_\infty\right)} \tag{12}$$

where, $\tau_\omega(x)$ is the shear stress, $q_\omega$ is the wall heat flux, and $q_m$ is the wall mass flux.

By applying the established definitions of the above quantities together with the previously introduced similarity transformations, the non-dimensional forms of $Cf_x, Nu_x, and\ Sh_x$ can be obtained as follows:

$$Cf_x\, Re_x^{1/2} = \frac{\mu_{hnf}\ /\ \mu_f}{\rho_{hnf}\ /\ \rho_f} f''(0)$$

$$Nu_x\, Re_x^{-1/2} = -\left(\frac{\kappa_{hnf}}{\kappa_f} + \frac{4}{3}R\right)\theta'(0)$$

$$Sh_x\, Re_x^{-1/2} = -\phi'(0) \tag{13}$$

where $Re_x$ is the local Reynolds number.

# 3. Computational Method

In this work, the shooting method is used to solve the boundary value problems (BVPs) derived from the governing ordinary differential equations. The approach converts the BVP into an equivalent initial value problem (IVP) by introducing unknown initial conditions. An initial estimate for these conditions is selected, and the IVP is then integrated—typically using a Runge–Kutta scheme. The resulting boundary value problem (BVP) is solved numerically using MATLAB's built-in ode45 solver. The resulting solution is evaluated against the boundary conditions at the terminal point. If the conditions are not met, the initial guesses are adjusted and the procedure is repeated until the required accuracy is obtained. To improve convergence, root-finding techniques such as the bisection, secant, or Newton methods are employed to systematically refine the estimates. This strategy provides an accurate and efficient means of computing solutions to the BVPs under consideration. Before solving the system with ode45, the governing higher-order equations are reduced to first-order ordinary differential equations through the introduction of auxiliary variables:

$$f = y_1, f' = y_2, f'' = y_3, f''' = y_4, f'^v = y_5, \theta = y_6, \theta' = y_7, \phi = y_8, \phi' = y_9$$

The reduced first order differential equations are:

$$y_1{}' = y_2$$
$$y_2{}' = y_3$$
$$y_3{}' = y_4$$
$$y_4{}' = y_5$$
$$y_5{}' = \frac{1}{k^*}\left[\frac{\mu_{hnf}}{\mu_f} y_4 + \frac{\rho_{hnf}}{\rho_f}\left(y_1 y_3 - y_2{}^2\right) - \frac{\sigma_{hnf}}{\sigma_f} M y_2\right]$$

$$y_6' = y_7$$

$$y_7' = -\frac{Pr}{\left(\frac{\kappa_{hnf}}{\kappa_f} + \frac{4R}{3}\right)}\left[\frac{\left(\rho C_p\right)_{hnf}}{\left(\rho C_p\right)_f} y_4 y_7 + \lambda y_6\right]$$

$$y_8' = y_9$$

$$y_9' = -Sc\left[y_1 y_9 - \Omega\left(y_6\gamma + 1\right)^n e^{-\frac{E}{(y_6\gamma+1)}} y_8\right] \tag{14}$$

The initial conditions take the form

$$\text{at } \eta = 0, y_1 = s, y_2 = 1 + \beta y_3, y_3 = p, y_4 = q, y_5 = r, y_6 = 1, y_7 = a, y_8 = 1, y_9 = b \tag{15}$$

Initializing with $y_3 = p, y_4 = q,\ y_5 = r,\ y_7 = a, y_9 = b$ , the iterations run until the criteria for far field the boundary conditions is met. The step size $\rho$ = 0.001 is used while obtaining the numerical solution with $\rho_{max}$=10. The Newton–Raphson scheme is employed to enforce the boundary conditions at infinity, providing quadratic convergence of the iterative process. The numerical results of this paper are calculated by using the error tolerance $\xi = 10^{-6}$. The typical computing time for the numerical simulations is on the order of seconds to a few minutes per run, depending on the parameter set. A detailed explanation of this algorithm is given in Gladwell and Sayers [46].

# 4. Code Validation

The accuracy and credibility of the present numerical methodology are established through a systematic validation against previously reported results, as documented in Table **3**. This table presents a comparative study of the surface heat transfer rate, represented by −θ'(0), for various values of the Prandtl number (Pr) in the case of regular fluids, alongside the results available in the literature by Ramzan *et al*. [47], Govardhan *et al*. [48, 49], and Srisailam *et al*. [50]. An excellent level of agreement is observed between the present results and the cited studies over the entire range of Pr considered. This close correspondence not only confirms the numerical accuracy of the proposed solution procedure but also substantiates the validity and robustness of the underlying mathematical formulation adopted in the present analysis.

**Table 3: Comparison of the values of *−θ'(0)* for different values of Prandtl number Pr in the absence of nanoparticles for the limiting case M=0, S=0, k*=0, Bi→∞.**

| Pr | Ramzan *et al*. [47] | Govardhan *et al*. [48] | Govardhan *et al*. [49] | Srisailam *et al*. [50] | Present Result |
|---|---|---|---|---|---|
| 0.70 | 0.4539 | 0.4539 | 0.4539 | 0.45391 | 0.453907 |
| 2.00 | 0.9114 | 0.9114 | 0.9114 | 0.91142 | 0.911424 |
| 7.00 | 1.8954 | 1.8954 | 1.8954 | 1.895421 | 1.835427 |

# 5. Results and Discussions

In the present study, the nanoparticle volume fractions $\varphi_1$ and $\varphi_2$ were varied in the range $0 \le \varphi_1, \varphi_2 \le 0.05$. This range is consistent with commonly reported values in the hybrid nanofluid literature and corresponds to dilute to moderately concentrated suspensions. Such low volume fractions are generally considered physically realistic, as they ensure stable dispersion of Cu and $Al_2O_3$ nanoparticles in the base fluid, minimize agglomeration and sedimentation, and avoid excessive increases in viscosity. Therefore, the chosen parameter ranges represent

practical and experimentally feasible conditions for maintaining the stability and effective thermal performance of hybrid nanofluids.

### 5.1. Impact of Magnetic Field

Fig. (**2a**) shows the velocity profiles for different values of the magnetic parameter M. It is clear that the fluid velocity decreases as M increases, both with and without velocity slip. This behaviour arises from the application of a transverse magnetic field, which induces a Lorentz force acting opposite to the direction of flow. This force behaves like a magnetic drag, suppressing the motion of the electrically conducting fluid and thereby reducing its velocity. As a consequence of this magnetic damping, the momentum boundary layer becomes thinner with increasing M; the fluid momentum diffuses less effectively away from the wall. This feature is significant in magnetohydrodynamic (MHD) technologies such as electromagnetic pumping, MHD ion propulsion, flow-control systems, and metallurgical processing, where magnetic fields are used deliberately to regulate or suppress flow.

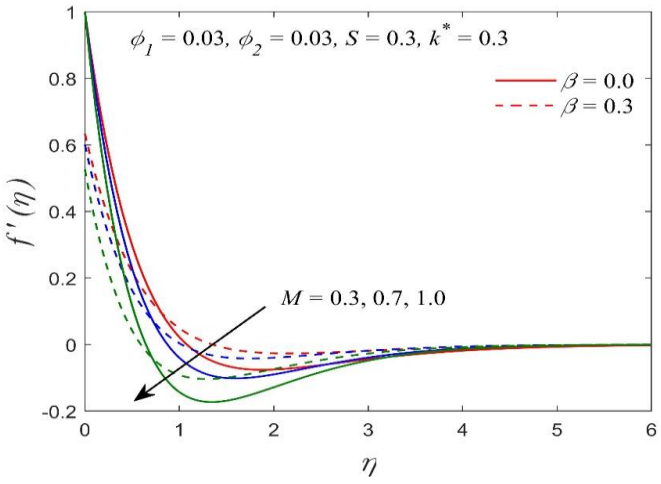


**Figure 2:** (**a**) Velocity profiles for different values of magnetic parameter.

Fig. (**2b**) illustrates the temperature distribution for various magnetic parameter values. The fluid temperature increases as M increases. When a magnetic field is applied, part of the mechanical energy lost due to magnetic damping converts into Joule (ohmic) heating**,** which raises the fluid temperature. This effect becomes more pronounced in hybrid nanofluids due to their enhanced thermal conductivity and stronger energy-diffusion capability, which collectively thicken the thermal boundary layer and promote a more uniform temperature distribution.

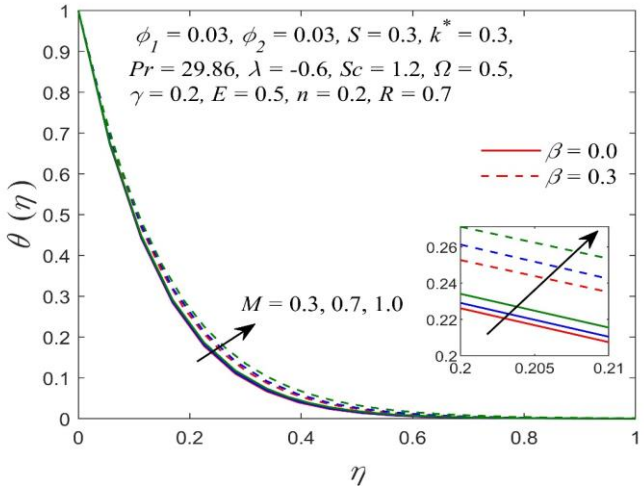


**Figure 2:** (**b**) Temperature profiles for different values of magnetic parameter.

Fig. (**2c**) indicates that the concentration profile increases with higher values of both the slip parameter and the magnetic parameter. An increase in slip reduces the near-wall mass flux, allowing species concentration to accumulate near the surface. Similarly, a higher magnetic parameter suppresses fluid motion, reducing convective mixing and enabling greater solute build up within the boundary layer. As a result, the concentration boundary layer becomes thicker with increasing M, reflecting weaker mass-diffusion transport.

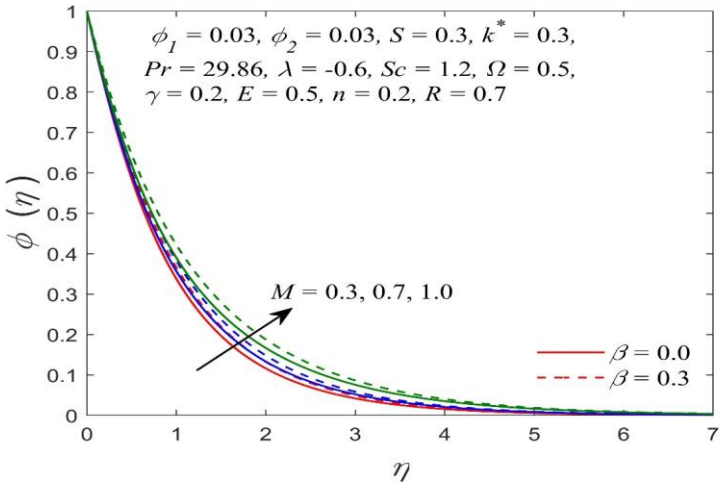


**Figure 2:** (**c**) Concentration profiles for different values of magnetic parameter.

The figures also reveal that as the slip parameter (β) increases, the temperature and concentration profiles rise, whereas the velocity along the stretched sheet decreases noticeably. The velocity initially decreases with an increasing slip parameter because larger slip reduces the shear transfer from the wall to the fluid. However, beyond a certain distance from the surface, the velocity becomes higher compared to the no-slip case. This occurs because slip conditions reduce near-wall resistance, allowing the core fluid to maintain higher momentum, which ultimately raises the velocity farther from the wall. Physically, this behaviour arises because a larger slip parameter reduces the interaction between the fluid and the surface. As surface friction decreases, the fluid moves more slowly. The diminished contact simultaneously reduces heat loss from the fluid, resulting in an elevated temperature. The rise in temperature increases molecular activity, which in turn boosts particle concentration near the sheet's surface. Consequently, the fluid's thermal characteristics are enhanced, and the particle distribution becomes more pronounced, creating a denser concentration region close to the surface.

### 5.2. Impact of Couple Stress Parameter

Fig. (**3a**) presents the variation of the velocity f'(η) with respect to the similarity variable η for different values of the couple-stress parameter $k^*$, while all other parameters are kept constant. The figure shows that increasing the couple-stress parameter enhances the velocity near the stretching surface. However, as the distance from the sheet increases, the velocity gradually decreases. This behaviour indicates that larger values of $k^*$ lead to a thicker momentum boundary layer. Physically, the presence of couple stresses introduces additional rotational and microstructural effects in the fluid, which enhance the momentum transfer close to the surface. As a result, the fluid experiences increased resistance to deformation, producing a thicker boundary layer. Thus, by adjusting $k^*$, the flow characteristics around the stretching surface can be effectively controlled.

Fig. (**3b**) and (**3c**) illustrate the temperature distribution θ(η) and concentration profile φ(η) for different values of the couple-stress parameter $k^*$. It is evident that both θ(η) and φ(η) decrease as the couple-stress parameter increases, and the corresponding thermal and concentration boundary layers also become thinner. Physically, this occurs because higher couple stresses enhance the rotational motion of fluid particles, which increases resistance to heat and mass diffusion. This reduces the ability of thermal energy and nanoparticles to spread away from the surface, resulting in lower temperature and concentration levels within the boundary layer. Consequently, stronger couple-stress effects suppress heat and mass transport, leading to thinner thermal and concentration boundary layers in the stretching sheet flow.

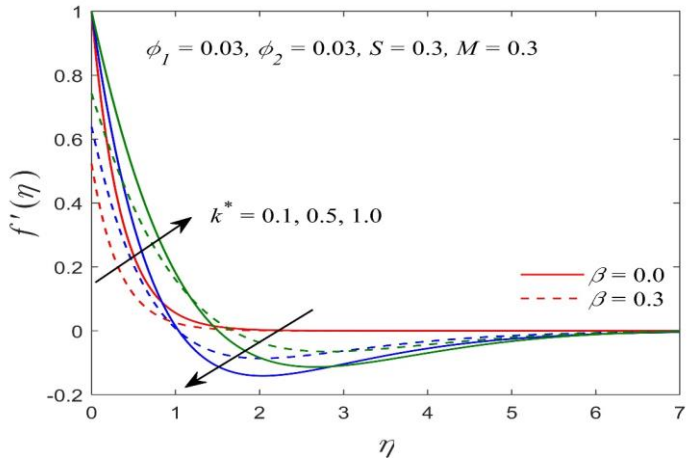


**Figure 3:** (**a**) Velocity profiles for different values of couple stress parameter.

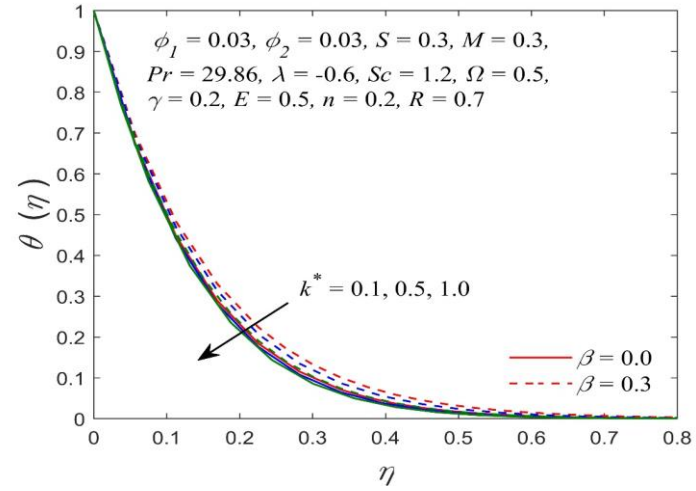


**Figure 3:** (**b**) Temperature profiles for different values of couple stress parameter.

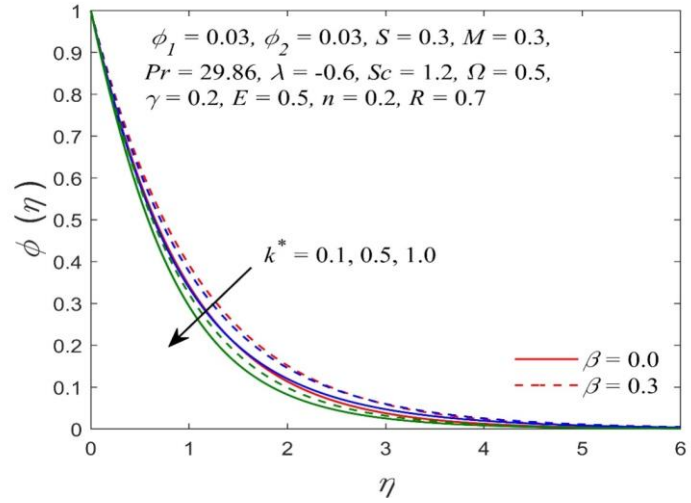


**Figure 3:** (**c**) Concentration profiles for different values of couple stress parameter.

### 5.3. Impact of Nanoparticle Volume Fractions $\phi_1$and $\phi_2$

The influence of the nanoparticle volume fractions $\phi_1$and $\phi_2$ on the temperature and concentration profiles is illustrated in Fig. (**4a**-**4d**). In this context, $\phi_1$ represents the volumetric concentration of $Al_2O_3$ (alumina oxide) nanoparticles, while $\phi_2$ denotes the volumetric concentration of Cu (copper) nanoparticles.

The temperature profiles shown in Fig. (**4a**) and (**4b**) clearly indicate that increasing either $\phi_1$ or $\phi_2$ leads to a rise in the temperature of the hybrid nanofluid. Physically, this behaviour can be attributed to the fact that introducing more nanoparticles enhances the effective thermal conductivity of the fluid. Silver nanoparticles, in particular, possess exceptionally high thermal conductivity; hence, their presence significantly improves the heat transport capability of the hybrid nanofluid. As a result, heat diffuses more effectively throughout the boundary layer, causing an overall elevation in temperature. However, Fig. (**4c**) shows that increasing $\phi_1$ leads to a reduction in the concentration profile near the stretching sheet. This can be explained by the fact that adding more $Al_2O_3$ nanoparticles increases the local particle-particle interactions and enhances Brownian motion. These effects accelerate the diffusion of nanoparticles away from the surface, reducing their concentration near the sheet. Additionally, higher nanoparticle loading increases mixture viscosity, which suppresses mass transfer close to the wall, resulting in a thinner concentration boundary layer. The concentration profile is observed to be an increasing function of $\phi_2$, the volume fraction of copper (Cu) nanoparticles (Fig. **4d**). This behaviour arises because increasing $\phi_2$ introduces a greater number of Cu nanoparticles into the fluid, thereby elevating the overall particle content within the boundary layer. Copper nanoparticles are relatively dense and possess strong thermal conductivity,

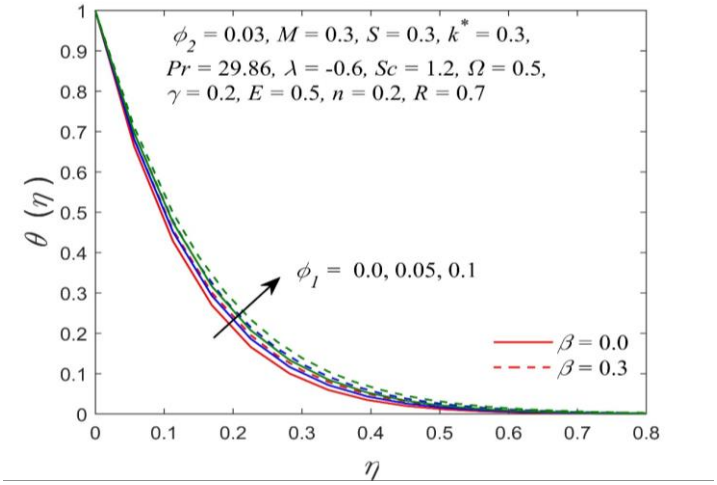


**Figure 4:** (**a**) Temperature profiles for different values of nanoparticle concentration $\phi_1$.

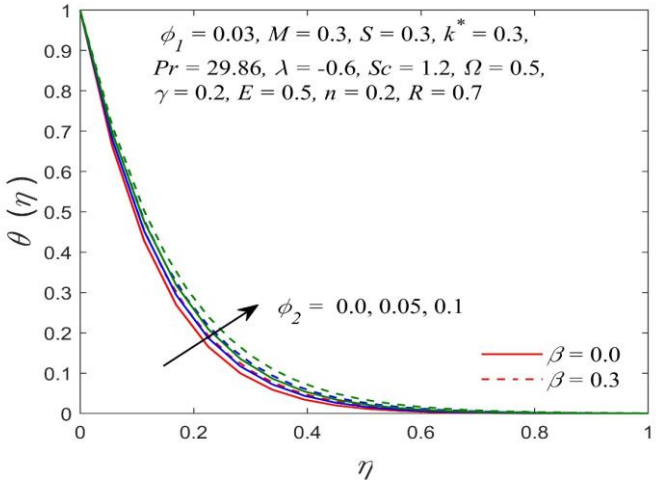


**Figure 4:** (**b**) Temperature profiles for different values of nanoparticle concentration $\phi_2$.

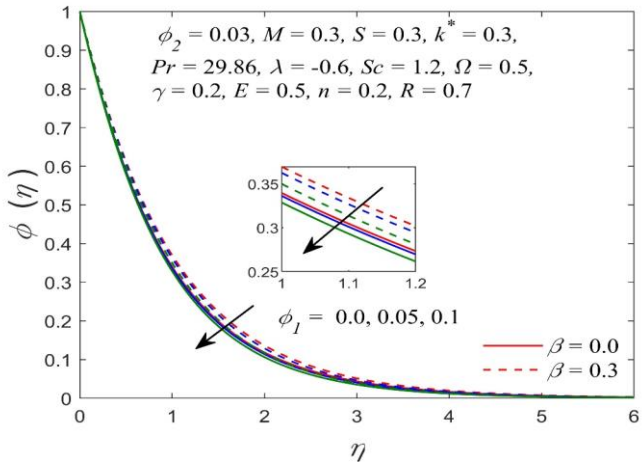


**Figure 4:** (**c**) Concentration profiles for different values of nanoparticle concentration $\phi_1$.

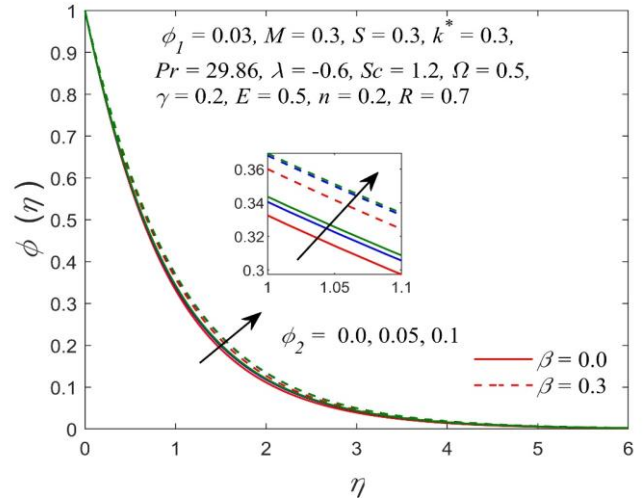


**Figure 4:** (**d**) Concentration profiles for different values of nanoparticle concentration $\phi_2$.

which slows their diffusion compared to lighter particles. As a result, these heavier nanoparticles tend to remain closer to the boundary layer region rather than dispersing rapidly into the fluid, leading to a thicker concentration boundary layer. Additionally, thermophoretic effects caused by temperature gradients can further accumulate nanoparticles near the surface, enhancing the concentration level. Therefore, the combined influence of higher particle loading, slower diffusion, and thermal-driven clustering results in a consistent increase in the concentration profile as $\phi_2$ increases.

### 5.4. Impact of Suction/Injection Parameter on Velocity

Fig. (**5**) illustrates how the velocity profiles of the couple-stress hybrid nanofluid vary with the similarity variable η for different values of the suction/injection parameter S in presence of velocity slip at the boundary. Positive values of S represent suction**,** meaning fluid is drawn toward the surface, whereas negative values indicate injection**,** where fluid is blown away from the surface.

The figure shows that increasing S (stronger suction) results in a noticeable decrease in the velocity field. The physical interpretation is as follows: Suction removes fluid from the boundary layer, causing the fluid near the surface to be more strongly attached to the sheet. This suppresses fluid motion, leading to a thinner boundary layer and lower velocity throughout the flow region. When velocity slip is present, the interaction between the fluid and the surface is already weakened. Therefore, the additional effect of suction further diminishes the fluid's

ability to move freely, resulting in a more pronounced decrease in velocity. Thus, the suction parameter provides an effective mechanism for controlling boundary layer thickness and velocity distribution in couple-stress hybrid nanofluids, with its influence amplified under slip conditions.

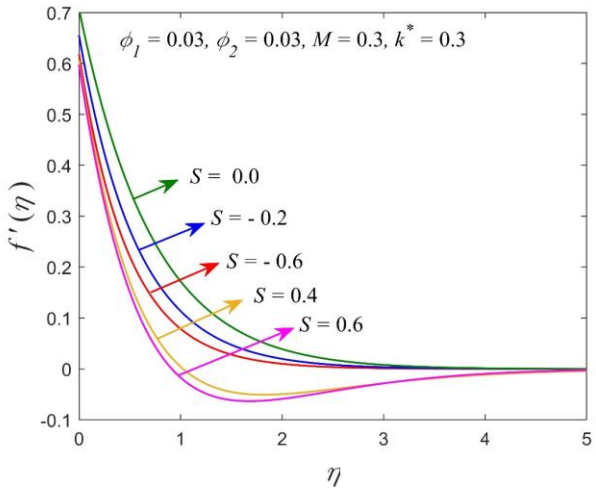


**Figure 5:** Velocity profiles for different values of suction and injection parameter.

### 5.5. Impact of Thermal Radiation on Temperature

The effect of thermal radiation on the temperature distribution of the hybrid Cu–$Al_2O_3$ nanofluid is investigated in the presence of magnetic field, slip conditions, couple stress effects, and chemical activation energy. Fig. (**6**) shows that as the radiation parameter increases, the temperature of the fluid rises throughout the boundary layer. Physically, this occurs because thermal radiation introduces additional energy into the fluid, enhancing thermal diffusion and counteracting the heat loss due to conduction.

In the context of magneto-radiative flows, the applied magnetic field induces a Lorentz force that tends to suppress the velocity field, which in turn reduces convective cooling and amplifies the temperature rise. Furthermore, the couple stress parameter increases fluid resistance, slowing the flow and allowing more time for the fluid to absorb radiative heat, while the activation energy affects reaction rates and can contribute to local heat generation. Overall, the combined effects lead to an increase in thermal energy with higher radiation intensity, which is critical for optimizing heat transfer applications in microscale and biomedical systems using hybrid nanofluids.

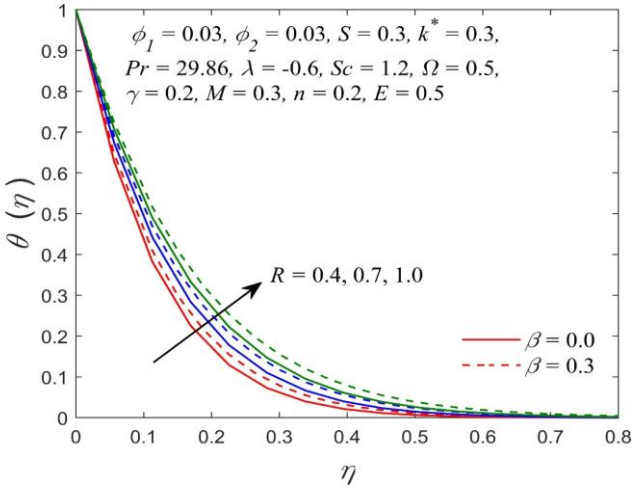


**Figure 6:** Temperature profiles for different values of thermal radiation parameter.

From an application standpoint, this behavior is significant in micro-scale cooling devices, biomedical hyperthermia treatments, and advanced thermal management systems, where controlling temperature profiles is critical. By increasing radiation, designers can enhance heat retention and thermal efficiency of hybrid nanofluids, making them suitable for high-heat flux environments and biomedical thermal therapies. Therefore, thermal radiation is a key parameter for optimizing both momentum and heat transfer in magneto-radiative slip flows of hybrid nanofluids.

### 5.6. Impact of Heat Source/Sink on Temperature

The presence of a heat sink (λ<0) significantly influences the temperature distribution within couple stress hybrid nanofluids, as illustrated in Fig. (**7**). A heat sink functions as a thermal energy extraction mechanism; therefore, an increase in the heat sink parameter intensifies the rate of heat removal from the fluid. Consequently, the temperature within the thermal boundary layer decreases. In couple stress hybrid nanofluids, this cooling effect becomes even more prominent due to the fluid's microstructural interactions and the enhanced thermal conductivity provided by the hybrid nanoparticles. This controlled cooling behaviour has important engineering applications. In microfluidic devices, heat sinks help prevent thermal overloading and ensure stable device operation. In industrial cooling systems, they enhance the efficiency of thermal management by dissipating excess heat from highly conductive hybrid nanofluids. Additionally, in high-performance thermal coatings and electronic cooling technologies, regulating the heat sink parameter enables precise temperature control, improving durability, performance, and reliability of thermal components.

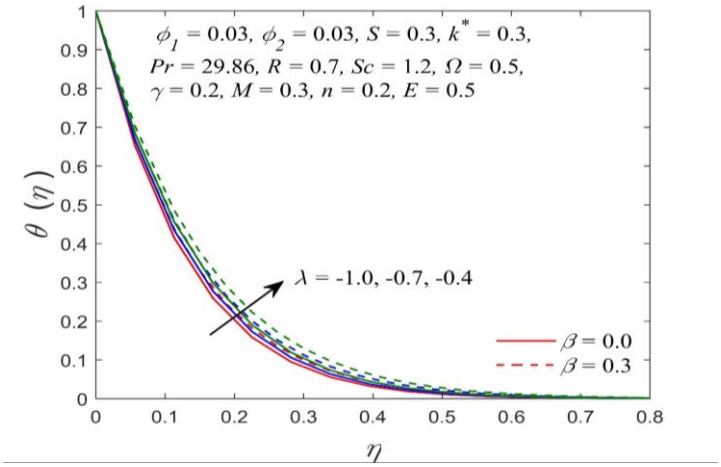


**Figure 7:** Temperature profiles for different values of heat sink parameter.

### 5.7. Impact of Activation Energy on Concentration

Fig. (**8**) illustrates the effect of the activation energy parameter E on the nanoparticle concentration distribution φ(η). It is observed that the concentration profile increases with increasing E. Physically, a higher activation energy represents a larger energy barrier that must be overcome for the chemical reaction to proceed. As a consequence, the reaction rate is reduced, leading to a lower consumption of reactant species within the boundary layer. This reduction in reaction intensity allows a greater amount of nanoparticles to remain suspended in the fluid, resulting in an enhanced concentration profile.

In the case of couple stress hybrid nanofluids, this phenomenon becomes more pronounced due to the presence of microstructural effects, which introduce additional resistance to molecular motion and suppress species diffusion. These effects further weaken the rate of mass transfer and reaction, thereby amplifying the accumulation of nanoparticles in the fluid. Moreover, the inclusion of velocity slip at the surface alters the mass transport mechanism near the wall. Slip reduces the shear interaction between the fluid and the surface, diminishing convective transport and facilitating the build-up of nanoparticles within the boundary layer. Consequently, the concentration enhancement associated with higher activation energy is more significant under

slip conditions compared to the no-slip case, where stronger fluid–wall interaction promotes mixing and slightly reduces the concentration growth.

These observations are particularly relevant in applications such as microreactors, chemical processing systems, thermal management devices, and biomedical transport processes, where precise control of activation energy and surface slip conditions can be utilized to regulate reaction rates and nanoparticle distribution.

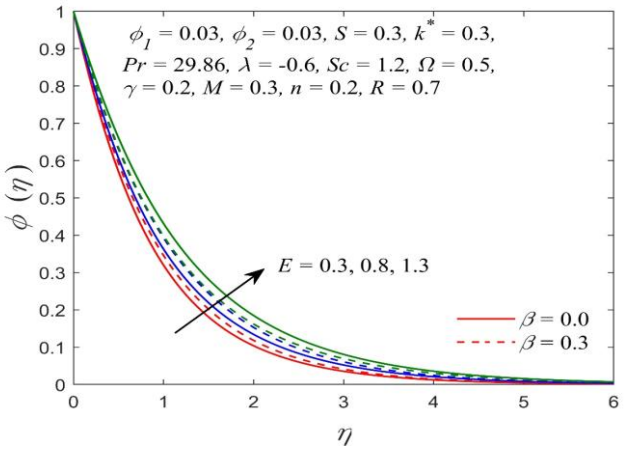


**Figure 8:** Concentration profiles for different values of activation energy parameter.

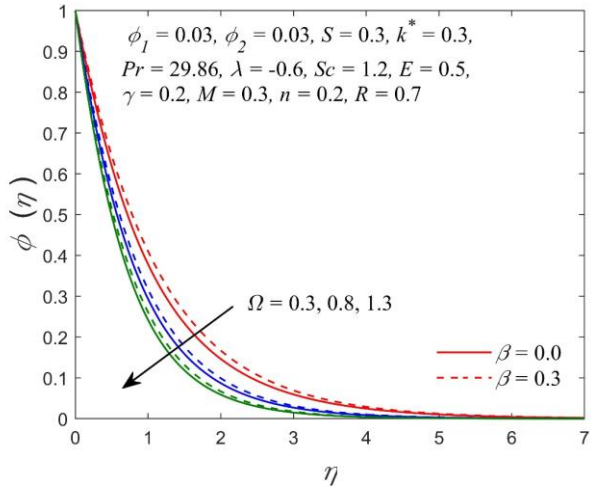


**Figure 9:** Concentration profiles for different values of chemical reaction parameter.

### 5.8. Impact of Chemical Reaction on Concentration

Fig. (**9**) illustrates the impact of the chemical reaction parameter (Ω) on the nanoparticle concentration profile, φ(η). The results show that as Ω increases, the concentration of the couple stress hybrid nanofluid decreases. For destructive (consumptive) reactions with Ω > 0, the chemical reaction actively removes nanoparticles from the fluid, leading to a noticeable reduction in concentration throughout the boundary layer, both with and without velocity slip. Physically, when the reaction rate becomes stronger than the rate at which nanoparticles are transported by diffusion and fluid motion, more nanoparticles are consumed than replenished. As a result, the concentration gradually decreases from higher to lower values across the flow region. This effect is observed similarly in both slip and no-slip conditions, although slip may slightly reduce shear at the surface, it does not alter the fundamental trend that stronger chemical reactions diminish nanoparticle concentration.This phenomenon has important practical implications in chemical reactors, microfluidic devices, drug delivery systems, and

hyperthermia treatments, where nanoparticle concentration directly affects heat transfer, chemical reaction rates, and therapeutic efficacy. Understanding the interplay of chemical reactions, slip effects, and nanoparticle dynamics allows for optimal control of thermal and mass transfer performance in engineering and biomedical applications.

### 5.9. Impact of Different Physical Parameters on the Skin Friction, the Nusselt Number and the Sherwood Number

Table **4** illustrates the influence of the nanoparticle volume fractions $\varphi_1$ and $\varphi_2$, slip parameter, magnetic parameter *M,* couple stress parameter *k*,* and suction parameter *S* on the skin-friction coefficient. In the absence of velocity slip, an increase in $\varphi_1$ and $\varphi_2$ leads to a noticeable rise in the magnitude of the skin friction. This behaviour is attributed to the enhanced effective viscosity and density of the hybrid nanofluid caused by the addition of nanoparticles, which intensifies momentum diffusion near the wall and consequently increases wall shear stress. However, when slip effects are present, the velocity gradient at the wall is reduced, weakening the fluid–surface interaction. As a result, increasing $\varphi_1$ and $\varphi_2$ under slip conditions leads to a reduction in the magnitude of the skin friction.

**Table 4: Behaviour of the skin friction for different values of the physical parameters.**

| $\varphi_1$ | $\varphi_2$ | $M$ | $k^*$ | $S$ | $Cf_x\,Re_x^{1/2}$ | |
|---|---|---|---|---|---|---|
| | | | | | $\beta = 0.3$ | $\beta = 0.0$ |
| 0.01 | 0.01 | 0.2 | 0.1 | 0.2 | -0.986138 | -1.656359 |
| 0.03 | | | | | -0.975737 | -1.666019 |
| 0.05 | | | | | -0.959611 | -1.6738 |
| | 0.03 | | | | -0.926343 | -1.623036 |
| | 0.05 | | | | -0.89568 | -1.58404 |
| | | 0.3 | | | -0.995228 | -1.705665 |
| | | 0.4 | | | -1.031807 | -1.828919 |
| | | | 0.35 | | -1.058578 | -1.807438 |
| | | | 0.4 | | -1.068721 | -1.870429 |
| | | | | 0.5 | -1.145759 | -1.890773 |
| | | | | 0.6 | -1.224768 | -2.004787 |

Furthermore, the magnitude of the skin friction is found to increase with rising values of the magnetic parameter *M.* This is due to the Lorentz force generated by the applied magnetic field, which opposes the fluid motion and produces an additional resistive force, thereby enhancing the shear stress at the surface. Similarly, an increase in the couple stress parameter *k** strengthens the microstructural effects within the fluid, resulting in greater resistance to deformation and hence a higher wall shear stress. In addition, higher suction parameter *S* draws the fluid closer to the surface, thins the momentum boundary layer, and intensifies the velocity gradient at the wall, leading to an increase in the skin-friction magnitude.

As shown in Table **5**, the Nusselt number increases with increasing nanoparticle volume fractions $\varphi_1$ and $\varphi_2$, magnetic parameter *M,* couple stress parameter *k*,* heat sink parameter, and radiation parameter. The rise in the Nusselt number with higher $\varphi_1$ and $\varphi_2$ is attributed to the enhanced effective thermal conductivity of the hybrid nanofluid, which strengthens heat transport from the surface. Increasing *M* and *k** suppresses fluid motion and thins the thermal boundary layer, resulting in a steeper temperature gradient at the wall. Moreover, the heat sink removes thermal energy from the fluid, while thermal radiation enhances radiative heat flux, both of which intensify the wall temperature gradient. Consequently, the combined effects of these parameters lead to an enhanced surface heat transfer rate, as reflected by the increased Nusselt number.

**Table 5: Behaviour of the Nusselt Number for different values of the physical parameters.**

| $\varphi_1$ | $\varphi_2$ | $M$ | $k^*$ | $S$ | $\lambda$ | $R$ | $Nu_x\, Re_x^{-1/2}$ | |
|---|---|---|---|---|---|---|---|---|
| | | | | | | | $\beta = 0.3$ | $\beta = 0.0$ |
| 0.01 | 0.01 | 0.2 | 0.2 | -0.1 | -0.3 | 0.4 | 3.600405 | 4.40236 |
| 0.03 | | | | | | | 3.665586 | 4.488363 |
| 0.05 | | | | | | | 3.730764 | 4.57435 |
| | 0.03 | | | | | | 3.800409 | 4.670024 |
| | 0.05 | | | | | | 3.869056 | 4.763798 |
| | | 0.3 | | | | | 3.879838 | 4.775715 |
| | | 0.4 | | | | | 3.891661 | 4.789812 |
| | | | 0.25 | | | | 4.031556 | 4.93561 |
| | | | 0.3 | | | | 4.188401 | 4.948026 |
| | | | | 0.0 | | | 5.952882 | 6.583681 |
| | | | | 0.1 | | | 7.797028 | 8.500739 |
| | | | | | -0.2 | | 7.357127 | 8.108265 |
| | | | | | -0.1 | | 6.885947 | 7.694208 |
| | | | | | | 0.7 | 7.318117 | 8.190654 |
| | | | | | | 1.0 | 7.70534 | 8.632461 |

Table **6** indicates that the Sherwood number decreases with increasing nanoparticle volume fractions $\varphi_1$ and $\varphi_2$, magnetic parameter, and activation energy. The addition of nanoparticles enhances the effective viscosity and thickens the concentration boundary layer, which weakens the concentration gradient at the wall and reduces mass transfer. Similarly, a stronger magnetic field suppresses fluid motion through the Lorentz force, while higher activation energy inhibits chemical reactions, both of which diminish species diffusion at the surface. In contrast, the Sherwood number increases with rising couple stress parameter $k^*$, Schmidt number $Sc$, and chemical reaction parameter, as these parameters reduce mass diffusivity, thin the concentration boundary layer, and intensify the concentration gradient at the wall, thereby enhancing the mass transfer rate.

# 6. Conclusion

Considering the effects of electro-magnetohydrodynamics, this study investigates the behaviour of a couple stress hybrid nanofluid flowing over a stretching sheet under a velocity slip boundary condition in the presence of thermal radiation. The hybrid nanofluid is formulated by dispersing two different types of nanoparticles—Copper (Cu) and Alumina ($Al_2O_3$)—into a base fluid consisting of an equal mixture (50%-50%) of ethylene glycol and water. The resulting Cu–$Al_2O_3$/ethylene glycol–water hybrid nanofluid is selected due to its superior thermal conductivity and strong chemical stability.

The influence of the governing parameters on the flow, thermal, and mass transport characteristics can be summarized as follows. An increase in the Hartmann number intensifies magnetic effects, leading to a suppression of fluid motion due to the Lorentz force, while simultaneously elevating the temperature and nanoparticle concentration distributions. The incorporation of velocity slip at the surface weakens the momentum transfer between the fluid and the wall, resulting in reduced velocity near the surface, accompanied by enhanced thermal and concentration fields. The application of suction or injection at the boundary significantly alters the flow structure; in comparison to impermeable surfaces, these conditions reduce velocity, temperature, and concentration profiles, whereas smoother and more uniform distributions are observed when mass transfer is absent. Furthermore, an increase in the couple stress parameter promotes fluid motion by enhancing the velocity

field, while diminishing the temperature and concentration profiles due to microstructural resistance effects. Finally, higher Schmidt number and chemical reaction parameter values suppress nanoparticle concentration, whereas elevated activation energy acts to increase the concentration distribution.

**Table 6: Behaviour of the Sherwood Number for different values of the physical parameters.**

| $\varphi_1$ | $\varphi_2$ | $M$ | $k^*$ | $S$ | $\lambda$ | $Sc$ | $E$ | $\Omega$ | $n$ | $Sh_x\, Re_x^{-1/2}$ | |
|---|---|---|---|---|---|---|---|---|---|---|---|
| | | | | | | | | | | $\beta = 0.3$ | $\beta = 0.0$ |
| 0.01 | 0.01 | 0.2 | 0.1 | -0.1 | -0.3 | 0.9 | 0.4 | 0.4 | 0.1 | 0.489961 | 0.55202 |
| 0.03 | | | | | | | | | | 0.487777 | 0.549088 |
| 0.05 | | | | | | | | | | 0.485613 | 0.546153 |
| | 0.03 | | | | | | | | | 0.483498 | 0.543463 |
| | 0.05 | | | | | | | | | 0.481388 | 0.540704 |
| | | 0.3 | | | | | | | | 0.481687 | 0.541179 |
| | | 0.4 | | | | | | | | 0.481997 | 0.541673 |
| | | | 0.2 | | | | | | | 0.515094 | 0.588724 |
| | | | 0.3 | | | | | | | 0.552418 | 0.621642 |
| | | | | 0.0 | | | | | | 0.646315 | 0.658311 |
| | | | | 0.1 | | | | | | 0.665295 | 0.698407 |
| | | | | | -0.2 | | | | | 0.665058 | 0.698237 |
| | | | | | -0.1 | | | | | 0.664788 | 0.698048 |
| | | | | | | 1.1 | | | | 0.750813 | 0.792635 |
| | | | | | | 1.3 | | | | 0.831297 | 0.881581 |
| | | | | | | | 0.6 | | | 0.784239 | 0.835479 |
| | | | | | | | 0.8 | | | 0.743653 | 0.795632 |
| | | | | | | | | 0.6 | | 0.825255 | 0.876308 |
| | | | | | | | | 0.8 | | 0.896903 | 0.94711 |
| | | | | | | | | | 0.3 | 0.892876 | 0.943504 |
| | | | | | | | | | 0.5 | 0.889003 | 0.940036 |

The present model is limited by assumptions of steady, two-dimensional laminar flow with constant properties, uniform nanoparticle dispersion, a uniform magnetic field, simplified thermal radiation and chemical reaction models, and the neglect of surface effects and geometric complexities, which may restrict its applicability to real-world systems.

# 7. Future Works

The present study is limited to steady, two-dimensional flow under simplified assumptions. Future work may extend the model to unsteady and fully three-dimensional flows to better represent transient and spatial variations found in practical applications. The fluid behaviour considered here represents a limited class of non-Newtonian models. Therefore, more general rheological models, such as Carreau, Cross, and Williamson fluids, can be examined to capture shear-dependent viscosity effects more accurately. In addition, the use of ternary hybrid nanofluids with three different nanoparticle types may be explored to further enhance thermal performance. Future studies may also consider complex geometries, porous or anisotropic media, and reactive flows to extend the applicability of the present model to practical thermal and engineering systems.

## Conflict of Interest

The authors declare no competing interests.

## Funding

The study received no external funding.

## Nomenclature

| | | |
|---|---|---|
| $B_0$ | = | Uniform magnetic field |
| $C$ | = | Fluid concentration (kg/m$^3$) |
| $Cw$ | = | Concentration at the surface (kg/m$^3$) |
| $Cp$ | = | Specific heat (J/kg K) |
| $C_\infty$ | = | Concentration far from the sheet(kg/m$^3$) |
| $Cf_x$ | = | Skin friction coefficient |
| $D_B$ | = | Brownian diffusion coefficient (m$^2$/s) |
| $E$ | = | Dimensionless activation energy |
| $E_a$ | = | Activation energy (kcal/mol) |
| $K$ | = | Thermal conductivity (W/m K) |
| $k^*$ | = | Couple stress parameter |
| $Kr$ | = | Chemical reaction rate |
| $L$ | = | Velocity slip factor |
| M | = | Magnetic parameter |
| $Nu_x$ | = | Nusselt number |
| Ω | = | Chemical reaction parameter |
| Pr | = | Prandtl number |
| R | = | Thermal Radiation parameter |
| $Re_x$ | = | Local Reynolds number |
| S | = | Suction / injection parameter |
| Sc | = | Schmidt number |
| $Sh_x$ | = | Sherwood number |
| $T$ | = | Temperature of the fluid (K) |
| $T_w$ | = | Temperature at the surface (K) |
| $(u,v)$ | = | (x,y) component of velocity(m/s) |
| $u_w$ | = | Velocity of the stretching sheet (m/s) |
| $v_w$ | = | Suction/injection parameter |

### Greek Symbols

$\phi_1, \phi_2$ = Nanoparticle volume concentration

$\rho$ = fluid density

$\lambda$ = Heat source/sink parameter

$\mu$ = Dynamic viscosity

$\sigma$ = Electric conductivity

$k$ = Thermal conductivity(W/m K)

$\Omega$ = Chemical reaction parameter

$\eta_0$ = Couple-stress viscosity

$B$ = Velocity slip parameter

$\theta$ = Fluid temperature

$\Phi$ = Fluid concentration

### Subscripts

$f$ = Base fluid

$nf$ = Nanofluid

$hnf$ = Hybrid nanofluid

# Reference

[1] Sakiadis BC. Boundary-layer behavior on continuous solid surfaces: II. The boundary layer on a continuous flat surface. AIChE J. 1961; 7(2): 221-5. https://doi.org/10.1002/aic.690070211

[2] Gupta PS, Gupta AS. Heat and mass transfer on a stretching sheet with suction or blowing. Can J Chem Eng. 1977; 55: 744-6. https://doi.org/10.1002/cjce.5450550619

[3] Rajagopal KR, Na TY, Gupta AS. Flow of viscoelastic fluid due to a stretching sheet. Rheol Acta. 1984; 23: 213-5. https://doi.org/10.1007/BF0133207

[4] Andersson HI. MHD flow of a viscoelastic fluid past a stretching surface. Acta Mech. 1992; 95: 227-30. https://doi.org/10.1007/BF01170814

[5] Mahapatra TR, Gupta AS. Heat transfer in stagnation point flow towards a stretching sheet. Heat Mass Transf. 2002; 38(6): 517-21. https://doi.org/10.1007/s002310100215

[6] Acrivos A, Shah MS, Petersson EE. Momentum and heat transfer in laminar boundary-layer flows of non-Newtonian fluids past external surfaces. AIChE J. 1960; 6(2): 312-7. https://doi.org/10.1002/aic.690060227

[7] Shenoy AV, Mashelkar RA. Thermal convection in non-Newtonian fluids. Adv Heat Transf. 1982; 15: 143-225. https://doi.org/10.1016/S0065-2717(08)70174-6

[8] Stokes VK. Couple stresses in fluid. Phys Fluids. 1966; 9(9): 1709-15. https://doi.org/10.1063/1.1761925

[9] Abbas T, Ahmad B, Khan SU, Haq EU, Hassan QMU, Wakij A. Couple stress flow of exponentially stretching sheet with Cattanco-Christor heat flux model. Heat Transf. 2022; 51(5): 4819-32. https://doi.org/10.1002/htj.22531

[10] Ali N, Khan SU, Sajid M, Abbas Z. MHD flow and heat transfer of couple stress fluid over an oscillatory stretching sheet with heat source/sink in porous medium. Alex Eng J. 2016; 55(2): 915-24. https://doi.org/10.1016/j.aej.2016.02.018

[11] Kumar M, Reddy G, Kumar N, Beg O. Application of differential transform method to unsteady free convective heat transfer of a couple stress fluid over a stretching sheet. Heat Transf. 2019; 48(2): 582-600. https://doi.org/10.1002/htj.21396

[12] Shah G, Rehman A, Sheikh N. Heat transfer analysis over the boundary layer stagnation-point flow of couple stress fluid over an exponentially stretching sheet. Am J Appl Math. 2022; 10(3): 100-5. https://doi.org/10.11648/j.ajam.20221003.13

[13] Hanif I, Ul Haq R, Alshomrani AS. Convective heat transfer of couple stress fluid flow with thermal radiation effect: dual nature study. Int Commun Heat Mass Transf. 2025; 169: 109906. https://doi.org/10.1016/j.icheatmasstransfer.2025.109906

[14] Choi SUS, Eastman JA. Enhancing thermal conductivity of fluids with nanoparticles. ASME FED. 1995; 231: 99-105.

[15] Rohinee B, Kumar D, Wankhade AV. Heat transfer performance of nanofluids in heat exchanger: a review. J Therm Eng. 2023; 9(1): 86-106. https://doi.org/10.18186/thermal.1243398

[16] Nabwey HA, Armaghani T, Azizimehr B, Rashad AM, Chamkha AJ. A comprehensive review of nanofluid heat transfer in porous media. Nanomaterials. 2023; 13: 937. https://doi.org/10.3390/nano13050937

[17] Das PK, Santra AK, Ganguly R, Dash SK, Muthusamy S, Sha M, *et al*. An extensive review of preparation, stabilization, and application of single and hybrid nanofluids. J Therm Anal Calorim. 2024; 149: 9523-57. https://doi.org/10.1007/s10973-024-13449-1

[18] Rasool G, Islam S, Hussain S, Sun T. Parametric analysis of heat and mass transfer in nanofluid flow through a porous channel with Brownian motion and thermophoresis effects. Int J Thermo-Fluid Syst Sustain Energy. 2025; 1(1): 16-29. https://doi.org/10.62762/IJTSSE.2025.261546

[19] Saraf AK, Goyal Y, Yusop AFR. Application of nanofluids under laminar flow regime in heat exchangers—a review. Discover Appl Sci. 2025; 7: 1154. https://doi.org/10.1007/s42452-025-07726-3

[20] Mezrakchi R Al. Investigation of various hybrid nanofluids to enhance the performance of a shell and tube heat exchanger. AIMS Energy. 2024; 12(1): 235-55. https://doi.org/10.3934/energy.2024011

[21] Ekiciler R. Performing $SiO_2$–MWCNT/water hybrid nanofluid with differently shaped nanoparticles to enhance first- and second-law features of flow by considering a two-phase approach. J Therm Anal Calorim. 2024; 149: 1725-44. https://doi.org/10.1007/s10973-024-12885-3

[22] Oladetan JO, Fujah FM, Omosehin OS, Atofarati EO, Nwabuko U, Olakoyejo OT, *et al*. Numerical investigation of heat transfer performance of hybrid nanofluid in porous substrate in microchannel heat sink. Int J Appl Comput Math. 2025; 11: 151. https://doi.org/10.1007/s40819-025-01973-z

[23] Kalsi S, Kumar S, Kumar A, Alam T, Sharma A, Yadav AS. A review on hybrid nanofluids for heat transfer: advancements, synthesis, challenges and applications. Discover Appl Sci. 2025; 7: 698. https://doi.org/10.1007/s42452-025-07141-8

[24] Gul T, Mukhtar S, Alghamdi W, Raizah Z, Alhazmi SE, Tageldin E. Frontiers in energy research. Front Energy Res. 2022; 10: 965309. https://doi.org/10.3389/fenrg.2022.965309

[25] Khashi NS, Hamzah KB, Waini I, Zainal NA, Arifin NM, Pop I. Magnetohydrodynamic couple stress hybrid nanofluid flow over a convectively heated stretching surface. Magnetohydrodynamics. 2024; 60(3-4): 197-206. https://doi.org/10.22364/mhd.60.3-4.3

[26] Motamari M, Pasupula M, Kumar N, Arvind HR, Vijayalakshmi R, Bhagya Lakshmi KV. Viscous dissipation and Joule heating effects on 3D couple stress nanofluid flow via stretching sheet. Int J Intell Syst Appl Eng. 2024; 12(22s): 1446.

[27] Khashi'ie NS, Hamzah KB, Mukhtar MF, Waini I, Pop I. Sensitivity analysis of the couple stress hybrid nanofluid flow over a stretchable plate with magnetic field. Math Model Comput. 2025; 12(2): 375-83. https://doi.org/10.23939/mmc2025.02.375

[28] Kakaç S, Pramuanjaroenkij A. Review of convective heat transfer enhancement with nanofluids. Int J Heat Mass Transf. 2009; 52(13-14): 3187-96.

[29] Chamkha AJ, Rashad AM. Magnetohydrodynamic hybrid nanofluid flow over a stretching sheet with thermal radiation and suction/injection. Appl Math Comput. 2013; 219(18): 9128-36.

[30] Davidson PA. Introduction to magnetohydrodynamics. Cambridge: Cambridge Univ Press; 2017.

[31] Hayat T, Nadeem S, Alsaedi A. MHD flow of hybrid nanofluid over a stretching sheet with heat transfer and suction effects. Appl Math Mech. 2016; 37(12): 1573-86.

[32] Mahdy AA, Abouelmagd A. Effects of magnetic field on hybrid nanofluid flow over a stretching sheet. Heliyon. 2020; 6(9): e04987.

[33] Khalili S, Dinarvand S, Hosseini R, Tamim H, Pop I. Unsteady MHD flow and heat transfer near stagnation point over a stretching/shrinking sheet in porous medium filled with a nanofluid. Chin Phys B. 2014; 23(4): 048203. https://doi.org/10.1088/1674-1056/23/4/048203

[34] Naramgari S, Sulochana C. Dual solutions of radiative MHD nanofluid flow over an exponentially stretching sheet with heat generation/absorption. Appl Nanosci. 2016; 6: 131-9. https://doi.org/10.1007/s13204-015-0420-z

[35] Reddy YD, Rao VS, Babu LAM. MHD boundary layer flow of nanofluid and heat transfer over a porous exponentially stretching sheet in presence of thermal radiation and chemical reaction with suction. Int J Math Trends Technol. 2017; 47(2): 87-100. https://doi.org/10.14445/22315373/IJMTT-V47P512

[36] Daniel YS, Aziz ZA, Ismail Z, Salah F. Thermal stratification effects on MHD radiative flow of nanofluid over nonlinear stretching sheet with variable thickness. J Comput Des Eng. 2018; 5(2): 232-42. https://doi.org/10.1016/j.jcde.2017.09.001

[37] Vishalakshi AB, Mahesh R, Mahabaleshwar US, Rao AK, Pérez LM, Laroze D. MHD hybrid nanofluid flow over a stretching/shrinking sheet with skin friction: effects of radiation and mass transpiration. Magnetochemistry. 2023; 9(5): 118. http://doi.org/10.3390/magnetochemistry9050118

[38] Fatunmbi EO, Are SO. Numerical investigation of MHD nanofluid flow over an exponentially stretching porous sheet with activation energy, chemical reaction, and non-uniform heat source. J Eng Res Rep. 2025; 27(6): 214-23. https://doi.org/10.9734/jerr/2025/v27i61539

[39] Mabood F, Yusuf TA, Bognar G. Features of entropy optimization on MHD couple stress nanofluid slip flow with melting heat transfer and nonlinear thermal radiation. Sci Rep. 2020; 10: 19163. https://doi.org/10.1038/s41598-020-76133-y

[40] Rajamani S, Subramanyam Reddy A. Effects of Joule heating and thermal radiation on MHD pulsating flow of a couple stress hybrid nanofluid in a permeable channel. Nonlinear Model Control. 2022; 27(4): 684-99. https://doi.org/10.15388/namc.2022.27.26741

[41] Shercliff JA. A textbook of magnetohydrodynamics. Oxford (UK): Pergamon Press; 1965.

[42] Brewster M. Thermal radiative transfer properties. New York: John Wiley and Sons; 1972.

[43] Raptis A. Radiation and free convection flow through a porous medium. Int Commun Heat Mass Transf. 1998;25(2):289-95.

[44] Srinivasa Reddy V, Kandasamy J, Sivanandam S. Joule heating, Dufour and Soret effects on MHD hybrid nanoliquid flow over a moving thin needle in a porous medium with thermal radiation. World J Eng. 2025; 22(4): 866-75. https://doi.org/10.1108/WJE-01-2024-0040

[45] Puneeth V, Manjunatha S, Makinde OD, Gireesha BJ. Bioconvection of a radiating nanofluid past a thin needle in the presence of heterogeneous–homogeneous chemical reaction. J Heat Transf. 2021; 143(4): 042502. https://doi.org/10.1115/1.4049844

[46] Gladwell I, Sayers DK. Computational techniques for ordinary differential equations. London: Academic Press; 1980.

[47] Ramzan M, Dawar A, Saeed A, Kumam P, Watthayu W, Kumam W. Heat transfer analysis of the mixed convective flow of magnetohydrodynamic hybrid nanofluid past a stretching sheet with velocity and thermal slip conditions. PLOS One. 2021; 16(12): e0260854. https://doi.org/10.1371/journal.pone.0260854

[48] Govardhan K, Narender G, Sarma GS. Viscous dissipation and chemical reaction effects on MHD Casson nanofluid over a stretching sheet. Malays J Fundam Appl Sci. 2019; 15(4): 585-92. https://doi.org/10.11113/mjfas.v15n4.1256

[49] Govardhan K, Narender G, Sarma GS. Heat and mass transfer in MHD nanofluid over a stretching surface along with viscous dissipation effect. Int J Math Eng Manag Sci. 2020; 5(2): 343-52. https://doi:10.33889/IJMEMS.2020.5.2.028

[50] Srisailam B, Sreeram Reddy K, Narender G, Malga BS. Flow and heat transfer analysis of MHD nanofluid due to convective stretching sheet. Indian J Sci Technol. 2022; 15(44): 2393-402. https://doi.org/10.17485/IJST/v15i44.1006